ACT Project Number:
271498

Project acronym:
ELEGANCY

Project full title:
Enabling a Low-Carbon Economy via Hydrogen and CCS

ERA-Net ACT project

Starting date: 2017-08-31
Duration: 36 months

D2.3.3
Direct spatial mapping of fracture properties during shearing displacements in rock cores

Actual Delivery date: 2018-12-10

Organization name of lead participant for this deliverable:
Imperial College London

ACT ELEGANCY, Project No 271498, has received funding from DETEC (CH), BMWi (DE), RVO (NL), Gassnova (NO), BEIS (UK), Gassco, Equinor and Total, and is cofunded by the European Commission under the Horizon 2020 programme, ACT Grant Agreement No 691712.		
Dissemination Level		
PU	Public	X
CO	Confidential, only for members of the consortium (including the Commission Services)	

Deliverable number:	D2.3.3
Deliverable title:	Report on single-phase core flooding experiments
Work package:	WP2 CO_2 transport, injection and storage
Lead participant:	ICL

Authors		
Name	**Organisation**	**E-mail**
Ronny Pini*	ICL	r.pini@imperial.ac.uk
Swapna Rabha	ICL	s.rabha@imperial.ac.uk
Claudio Madonna	ETH/SCCER	claudio.madonna@erdw.ethz.ch
Quinn Wenning	ETH/SCCER	quinn.wenning@erdw.ethz.ch

*Mark Lead author with asterisk

Keywords

Shearing, fracture, granite, petrophysics, core-analysis

Abstract

Within ELEGANCY, a new decameter-scale experiment is being conducted at the Mont Terri Underground Research Laboratory (URL) in Switzerland aimed at investigating the migration of CO_2-rich brine through a damaged zone within faults. One of the questions being addressed with this experiment is to what extent slip movements associated with the shearing of fractures can create permeable paths through the rock mass. We present here the results of an experimental campaign aimed at investigating shearing displacements in a Westerly granite rock core using a novel X-ray transparent shear-displacement core-holder. The displacement process is monitored in-situ enabling precise reconstruction of fracture aperture maps as a function of displacement (0 – 5.75 mm) at sub-millimeter resolution. We observe that shearing increases the core-averaged fracture aperture and broadens significantly the distribution of local values, which becomes strongly tailed towards large apertures as shearing progresses. While the correlation length of the aperture field increases in both parallel and perpendicular directions, significant anisotropy is also developed with the progression of shearing. These observations have bearing on the migration of fluids through fractured rocks and confirm the importance of considering the magnitude of micro-seismicity when estimating permeability enhancement due to shear displacement. The results also represent a benchmark for the next experimental campaign that will focus on samples from the Swiss subsurface, including the Opalinus clay from the Mont Terri underground research laboratory and the Muschelkalk limestone. For the latter, results from petrophysical analyses are also presented in this report.

TABLE OF CONTENTS

Page

1. INTRODUCTION

The hydromechanical coupling between flow and stresses in fractures has bearing on the understanding of natural processes (e.g., fault rupture) and on the design of reservoir engineering technologies, including oil and gas extraction, geothermal energy utilization and geological carbon storage. However, fluid transport through fractures is still far less understood than flow in porous media, limiting our ability to achieve the level of control that is required for any engineering application aimed at exploiting fracture media. One of the main challenges is that, in addition to the subsurface stress conditions, flow pathways through a fracture depend on its geometry, the magnitude and distribution of its aperture, as well as the structural and chemical heterogeneity of its surfaces. Recent results from a series of controlled water injection tests conducted at Mont Terri Underground Rock Laboratory (URL) in Switzerland indicate that sub-millimeter slip movements (0.01 – 0.1 mm) can create permeable paths across a fault-zone without producing significant seismic activity (Guglielmi et al. 2017). To improve our ability to predict fluid flow and stress perturbations in the subsurface, a better understanding is required of the processes that induce changes to fracture characteristics and of their implications.

Within ELEGANCY, a new decameter-scale experiment is being conducted at the Mont Terri URL in Switzerland aimed at investigating the migration of CO_2-rich brine through a damaged zone within faults. Two aspects are of particular interest to this project: (i) the shearing process, which can be a significant source of fracture permeability change, by altering the distribution of contact area and void space within the fracture itself; (ii) the interaction (or lack thereof) of the CO_2-rich brine with the surrounding environment that may provide additional control on the mobility of CO_2 within caprocks. Both aspects are currently being investigated as part of the ELEGANCY project.

This document is divided into two parts and builds on the findings from the two previous technical reports, where the results have been presented of the initial selection (D2.3.1 *Rock and fluid sample selection for petrophysics* studies) and characterization of rock samples (D2.3.2 *Pore and gas sorption properties of Opalinus Clay*). In this document, the results are presented of the experimental campaign aimed at investigating shearing displacements in a crystalline rock core using a novel X-ray transparent shear-displacement core-holder. The results represent a benchmark for the next experimental campaign that will focus on samples from the Swiss subsurface, including the Opalinus clay from the Mont Terri underground research laboratory and the Muschelkalk limestone. For the latter, results from petrophysical analyses are also presented in the second part of this report.

2. MATERIALS

Westerly granite was used in the experimental campaign. The rock is made up of quartz (27 vol%), plagioclase (30 vol%), microcline (36 vol%), phyllosilicates (6 vol%), and trace minerals (1 vol%) with homogeneously distributed grains (average grain size of 0.75 mm) (Meredith & Atkinson 1985). The sample was cored from a larger block to yield a cylindrical specimen with a diameter of 5 cm and a length of 10 cm. A single rough-walled fracture was induced along the length of the sample using the so-called Brazilian method (Wenning 2018). The test was modified to assist single fracture development by pressing wedges against diametrically opposite sides of the core that had a 1 mm deep etched groove to initialize the fracture. After the tensile fracture was induced, 2 cm of rock were trimmed from diagonally opposite sides of the core, so that the shearing can begin from a mated position.

3. IN-SITU DIRECT-SHEAR EXPERIMENTS

Changes in fracture aperture as a function of shear offset of the fracture plane were quantified using a X-ray transparent core holder designed in-house (Figure 1). The core-holder was designed and built at ETH Zurich. It consists of an aluminum pressure vessel that houses the fractured sample between a fixed end-cap at the lower assembly and an adjustable end-plate in the upper assembly. The latter enables using samples of variable length (7–12cm) in the core holder. A hollow aluminum spacer piston is fastened to the top of the upper end-cap so that the plumbing system can connect to the upstream side of the core. The hollow aluminum spacer is then connected in series to the load cell and the screw type displacement press that is mounted to the end plate of the upper assembly. Additional details on the direct-shear apparatus are provided in Wenning (2018).

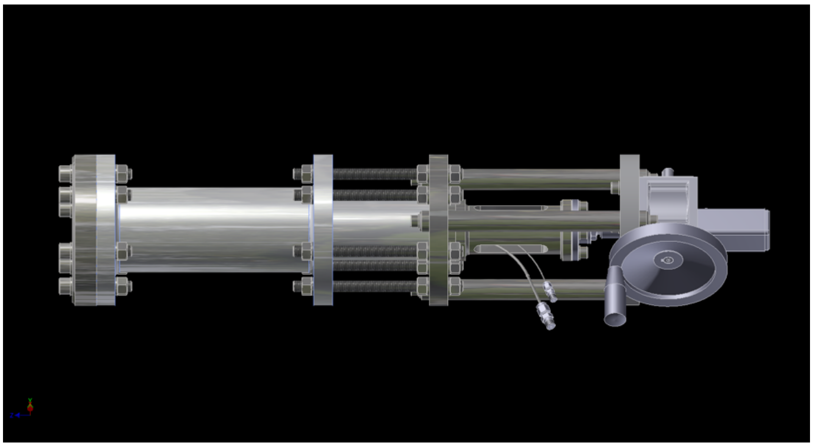

Figure 1 – Schematic of the direct shear apparatus for the experiments carried out as part of this study.

The experiment started with an initial confining pressure load up to 10 MPa using a high precision syringe pump (Teledyne ISCO, model 1000D). Air at atmospheric pressure was used as the pore fluid to create sufficient X-ray attenuation contrast between the rock matrix and the fracture. The shearing experiment started by reducing the confining pressure to 1.5 MPa and by maintaining it at this level using the syringe pump. Increments of 0.25 to 1 mm shear displacement were imposed using the 25 kN press until a maximum shear displacement of 5.75 mm was achieved. At each step, X-ray CT scans were acquired using the Toshiba Aquilion CT imager hosted in the Qatar Multiscale Imaging Lab at Imperial College London. The imaging parameters used throughout the study are: source voltage of 120 kV, tube current of 200 mA and voxel resolution of (0.113×0.113×1) mm^3. Scanning around the steel protectors that surround the sample and spacers leaves a 5 cm-long field of view around the center of the core. For image analysis the X-ray tomograms are resampled to a resolution of (0.226×0.226×1) mm^3 using in-house MATLAB routines.

To construct the fracture aperture maps the so-called Calibration-Free Missing Attenuation method was deployed (Huo et al. 2016). Briefly, for each two-dimensional tomogram, the fracture aperture at each location within the fracture plane is computed using the following equation:

$$d = \frac{R \sum_{i=1}^{N_{\mathrm{vox}}} (CT_{\mathrm{mat}} - CT_i)}{CT_{\mathrm{mat}} - CT_{\mathrm{air}}}$$

where d is the local fracture aperture, R is the voxel side-length (0.226 mm), CT_i is the measured attenuation is Hounsfield units at a location i along the line traversing the fracture. As shown in the equation, the number of voxels used for calculating the fracture aperture is N_{vox}. In fact, although the actual aperture of the fracture may be below the instrument's spatial resolution, the loss in attenuation of the X-ray beam due to its presence is smeared into a given number of neighboring voxels. For Westerly granite, this region was found to be N_{vox}= 11 and 23 voxels wide for low and high displacement experiments. Accordingly, CT_{mat} is defined by averaging a given set of the matrix voxels located beyond the region affected by the smearing of the attenuation and represents the reference baseline value. CT_{air} represents the second reference value corresponding to the beam attenuation in air (CT_{air} = -1000 HU).

Local fracture apertures are obtained by applying the equation above, while slice- and core-averaged apertures are computed by averaging these local values. We note that assuming a uniform matrix introduces a systematic error in the estimated fracture aperture that varies from 35 to 65 μm for a fracture zone of 11 and 23 voxels, respectively.

4. RESULTS OF DIRECT-SHEAR TESTS

Figure 2 displays the evolution of the fracture aperture field in three-dimensions at 0, 1, 3, and 5.75 mm displacement. A clear evolution is observed from a fairly uniform low aperture field in the mated configuration to a highly heterogeneous distribution of local fracture apertures with the progression of shearing. Moreover, after 1 mm offset a continuous growth of local apertures is observed, with regions of low and high aperture that broadly align perpendicular to the shearing direction. The core-averaged aperture increases from 0.069 ± 0.035 mm in the mated state (0 mm displacement) to 1.028 ± 0.065 mm at a displacement of 5.75 mm.

The histogram plots corresponding to each fracture map are also shown in Figure 2. At 0 mm shear displacement the fracture aperture distribution forms a relatively narrow normal distribution. As the fracture is progressively sheared from 1 mm onwards, the histograms evidence a significant broadening of the distribution of local apertures. Notably, the distributions show a characteristic tailing towards large values, with local fracture apertures reaching values as large as 3 mm.

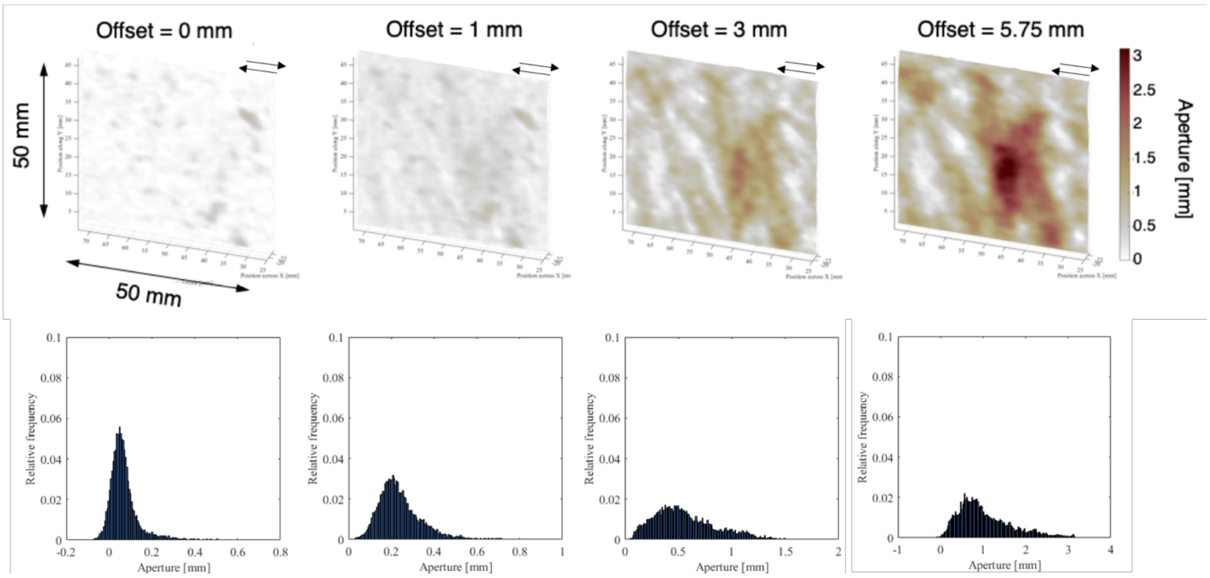

Figure 2 – *Top panel*: Three-dimensional fracture aperture maps for Westerly granite at various offset shear displacement (0 to 5.75 mm). Arrows indicate the shearing direction and the color-bar represents the aperture magnitude. *Bottom panel*: Histograms representing the fracture aperture distribution at various levels of shear displacement.

We have estimated the effects of shearing on other fracture properties, including contact area and fracture volume. The latter increases progressively from 162 ± 82 mm^3 (mated state) to 2404 ± 152 mm^3 (5.75 mm displacement), thereby supporting the progressive growth of the average fracture aperture discussed above. In terms of contact area between the two fracture planes, a drastic decrease (80 to 4 %) is observed between 0 mm and 1mm displacement and a small reduction is observed from 1 mm (4%) to the maximum displacement of 5.75 mm (1%). Gouge material formed by the wear at contacting asperities was observed on the fracture surfaces after the experiment. Notably, the spatial distribution of the gouge area observed in the photograph of the fracture surface matches well with the distribution of low aperture regions observed in the fracture aperture maps reconstructed from the CT tomograms.

In Figure 3 are shown experimental semi-variograms computed at 0, 1, and 5 mm displacement, which have been normalized with the variance of the log-transformed aperture distribution. These have been computed in the direction parallel (open symbols) and perpendicular to the shearing direction (closed symbols). Distinct curves are obtained at various level of shearing, reflecting changes in the correlation structure of the fracture aperture field. With increasing level of shearing, differences are also observed between curves computed in the two directions, indicating the creation of anisotropy. The values of core-averaged fracture apertures computed in the direction perpendicular and parallel to shearing support this observation. In particular, the computed anisotropy ratio $d_{\mathrm{pl}}: d_{\mathrm{pp}}$ decreases from 1.1 to 0.90 for the range of displacements considered in this study, indicating a significant increase in the aperture field in the direction perpendicular to shearing. The experimental semi-variograms have been fitted using the following exponential model:

$$\gamma_i(h) = C_i[1 - \exp(-3h/a_i)]$$

where i is the direction used for calculating the semi-variogram (i = pl or pp), h is the lag or distance separating two voxels, $C_i = \gamma_i(h \to \infty)$ is the sill or plateau that the semi-variogram develops when the data are no longer autocorrelated. The range, a_i, is the lag distance where the semi-variance approaches the sill, indicating the limiting 'spatial correlation length' where apertures are correlated to each other. The two parameters C_i and a_i are obtained by fitting the model to the experimental data.

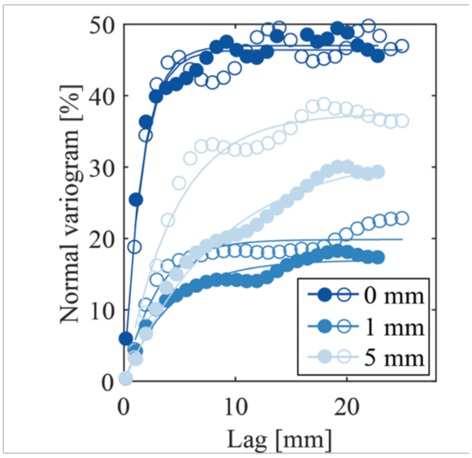

Figure 3 – Semi-variograms at 0, 1 and 5 mm shear displacement. The colors refer to a specific displacement with open and closed markers indicating the direction parallel and perpendicular to shearing, respectively. The solid lines are fits of the exponential model to each individual variogram.

It can be seen that this model provides a satisfactory fit of the experimental data. We observe that the maximum sill value is observed in the mated state ($C_{\mathrm{pl}} \approx C_{\mathrm{pp}} \approx 45\%$). The fact that this value is reached at short lag distances in both directions ($a_{\mathrm{pl}} \approx a_{\mathrm{pp}} \approx 5$ mm) further indicates low anisotropy and small correlation length in aperture values. Notably, the correlation length obtained in the direction perpendicular to shearing is systematically larger than the corresponding value computed in the direction parallel to shearing, confirming the appearance of anisotropy in the fracture aperture field. At a displacement of 5 cm, $a_{\mathrm{pl}} \approx 15$ mm $< a_{\mathrm{pp}} \approx 30$ mm. The correlation structure of the fracture aperture field suggests that, as the fracture continues to shear, the opening of the fracture allows for more correlation in the aperture and for an increased anisotropy within the fracture. Our experiments show that large fracture offset can increase the correlation length of aperture, even in the direction parallel to shearing. The latter could result in a better connectivity of flow pathways at larger displacements.

5. CHARACTERISATION OF MUSCHELKALK LIMESTONE

In the following, results are presented from the petrophysical analysis carried out on Muschelkalk Limestone provided by the Swiss partners in ELEGANCY (ETH/SCCER). We have deployed different laboratory techniques, including steady-state gas permeametry and porosimetry, Mercury intrusion porosimetry and X-ray imagery using both micro- and medical computed tomographic instruments. These have been used to quantify the porosity and pore-interconnectivity, permeability and capillary pressure curves. The workflow deployed for this experimental campaign is shown in Figure 4.

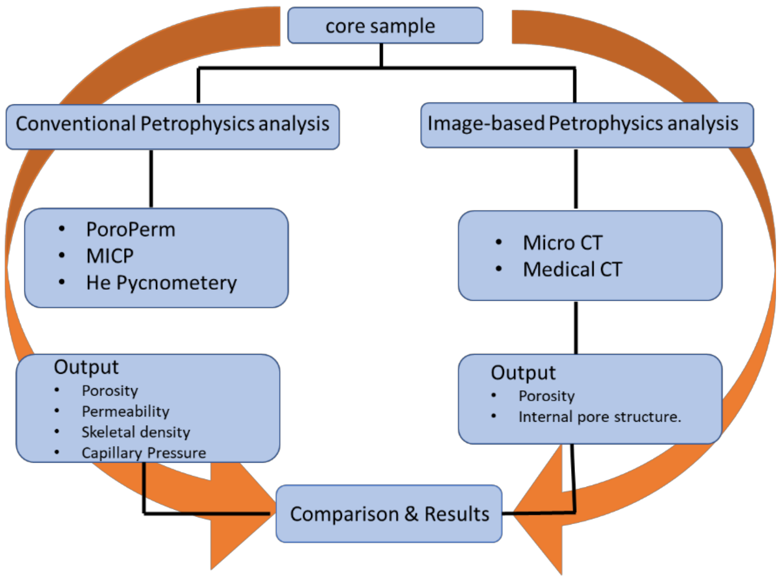

Figure 4 – Workflow deployed for the petrophysical characterization of Muschelkalk limestone.

5.1 Core-sample preparation

Figure 5 shows a digital photograph of the mother 9-cm diameter rock core together with the corresponding image obtained by X-ray CT (cross-section along the core length). This initial scan proved to be very useful to select the locations for obtaining sub-samples for subsequent analyses. In particular, four 3.8 cm – diameter cores were drilled from the main core, in addition to two smaller 1 cm – diameter plugs (Table 1). The naming convention used in this work for the five samples is Sample 2 through 6. Their dimensions and use within the experimental campaign are detailed in Table 1.

Table 1: The details of the core samples used in this core characterization study.

Core samples	Diameter (mm)	Length (mm)	Weight (gm)	Applied for
Sample 2	38.10	65.40	185.00	POROPERM
Sample 3	38.10	45.20	127.89	POROPERM
Sample 4	38.10	24.29	67.15	POROPERM
Sample 5	9.56	8.05	1.430	MICP, MicroCT
Sample 6	9.56	7.97	1.392	MICP

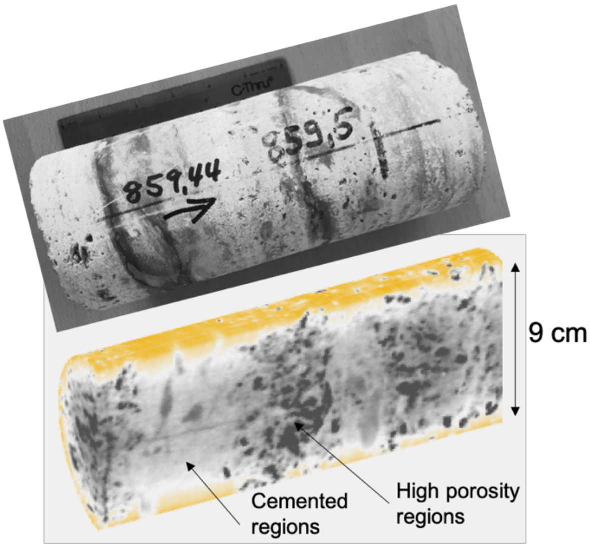

Figure 5 – The Muschelkalk limestone core used for petrophysical characterization: digital photograph (*top*) and reconstructed X-ray CT image (*bottom*).

5.2 Steady-state gas permeametry and porosimetry

The porosity and gas permeability of the carbonate rock sample 2, 3, and 4 were measured by the steady-state gas permeameter and porosimeter (POROPERM, Vinci Technologies). In these tests, porosity and permeability estimates are obtained from an isothermal nitrogen expansion experiment. The equivalent liquid permeability and slip are obtained by linear interpolation. Figure 6 shows digital photographs of the samples used in the analysis (vugs are also indicated by the blue circles) and Table 2 summarizes the obtained results.

Sample 2 Sample 3 Sample 4

Figure 6 – Samples used for permeability studies.

Table 2: Porosity and permeability values of Muschelkalk limestone.

	Sample 2	Sample 3	Sample 4
Porosity (-)	0.061	0.117	0.119
Gas permeability (mD)	0.093	0.096	0.194
Liquid permeability (mD)	0.057	0.057	0.120

As it can be seen from the table, the obtained permeability values are quite low (0.1–0.2 mD), while low to moderate porosities are observed (6–12%), despite the presence of relatively large vugs visible on the surface of the samples. These results suggest that pore-connectivity in this rock may be fairly low. This issue is further addressed by analyzing the small plugs.

5.3 Pore-structure analysis by micro-CT

Pore scale images of Sample 5 were captured using the micro-CT equipment (Vers500, Zeiss) at Imperial College London. For the measurements, the voltage and power of the X-ray source was set at 80 kV and 7W, respectively. Images were acquired at a resolution of 10.232 µm with 1s exposure time per projection. The fan beam angle used in the experiment was 17.86 deg and a 0.4X magnification was used to obtain pore scale images of 1000^3 voxels. Image analysis was carried out using Avizo 9.7.0 software. Gray-scale cross-sectional images of the Muschelkalk limestone sample are shown in Figure 7 at three different axial locations along the length of the sample.

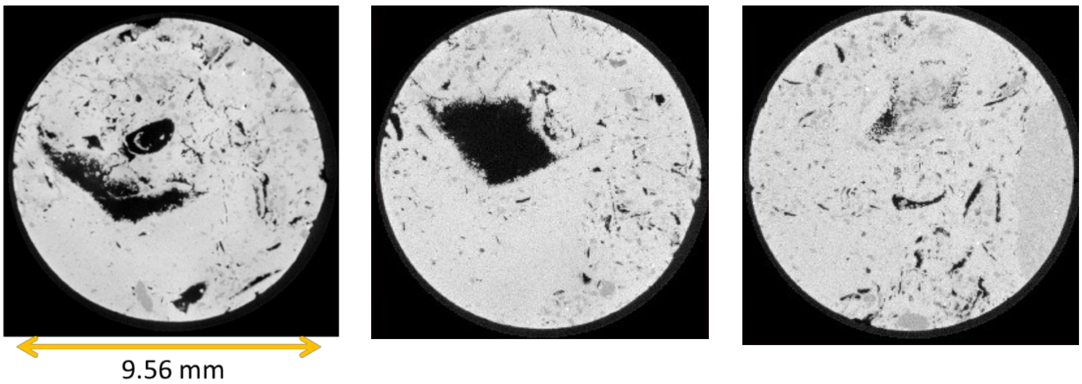

Figure 7 - Two-dimensional cross-section micro-CT images of the Muschelkalk limestone sample 5 at different axial positions. Pore-space is shown as black. Voxel resolution = 10µm.

Non-local means filter was used to improve the signal-to-noise ratio of the images, so as to enable a segmentation of the image into pore and grain phases. To this aim, interactive thresholding was used to obtain a binary image (Figure 8). Additional details of the image segmentation procedure used in this work can be found in Shah et al. (2016). The resolved porosity of the core sample is calculated from the segmented images as the ratio of the total number of pore voxels (i.e. in blue color in Figure 8) to the total number of voxels in the image (white + blue colors in Figure 8). The obtained porosity of the sample is 6.1 %, which agree with the value obtained for Sample 2 using N_2 porosimetry. Notably, the micro-CT images evidence the presence of large isolated pores, thus supporting the fairly low measured permeability values.

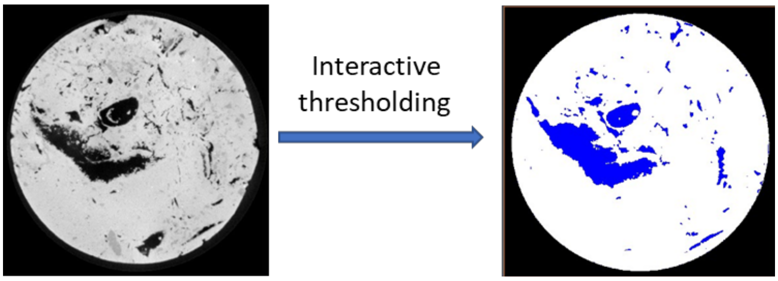

Figure 8 – Image segmentation of a reconstructed tomogram to a binary image for volume fraction calculation.

5.4 Capillary pressure curve analysis

Capillary pressure curves were measured on Sample 5 and Sample 6 by Mercury Intrusion Porosimetry (MIP, using the Autopore IV 9500 by Micromeritics) in the pressure range vacuum to 230 MPa. The obtained curves are shown in Figure 9 in terms of applied (capillary) pressure as a function of the intruded mercury saturation.

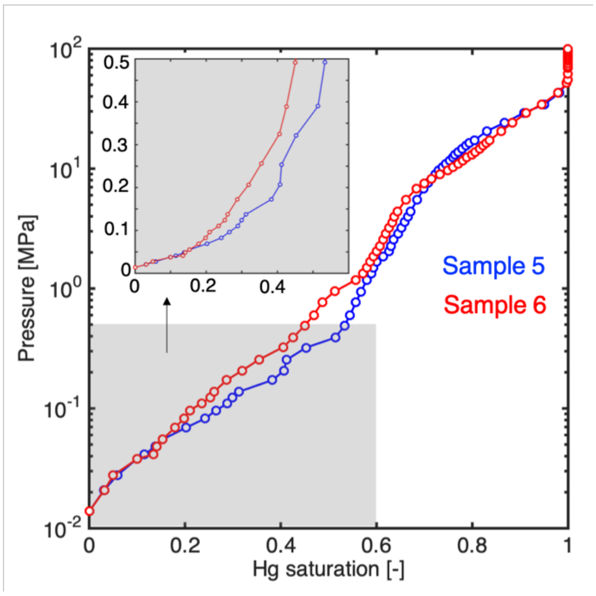

Figure 9 – Capillary pressure curves measured by MIP on sample 5 (blue) and 6 (red). In the inset the same data are presented in the pressure range 0 – 0.5 MPa.

The curves measured on the two sample show a very similar behavior characterized by a gradual increase of mercury saturation with increasing pressure. The absence of a clear plateau indicates that the pore space is largely heterogeneous with a wide range of pore-sizes. From the curves, estimates for the bulk density, skeletal density and porosity of the samples are obtained (data summarized in Table 3). It can be seen that the obtained porosity values agree fairly well with independent estimates from N_2 porosimetry and image analysis on microCT scans discussed above.

Table 3: Properties of Muschelkalk limestone estimated from MIP

	Sample 5	Sample 6
Porosity (-)	0.091	0.087
Bulk density (g/mL)	2.464	2.552
Skeleton density (g/mL)	2.711	2.795

6. CONCLUDING REMARKS

A newly designed X-ray transparent core-holder was used to study the evolution of the fracture aperture field of Westerly granite undergoing shear displacement. We observe a continuous increase in the core-averaged mechanical aperture of the fracture from 0–5.75 cm shear displacement. Notably, the shearing not only changes the fracture aperture, which alters the fracture volume, but also significantly reduces the contact area of the fracture and creates anisotropy in the distribution of apertures. The results represent a benchmark for the next experimental campaign that will focus on samples from the Swiss subsurface, including the Opalinus clay from the Mont Terri underground research laboratory and the Muschelkalk limestone. For the latter, results from petrophysical analyses have also been presented in the second part of this report. The pore-space of the Muschelkalk limestone sample is characterized by low connectivity and by a wide range of pore-sizes. The rock possesses fairly low permeability (0.05 mD ~ 0.12 mD) and low-to-moderate porosity (6.1 -12%). For the porosity independent observations have been obtained using three techniques, namely N_2 porosimetry, mercury intrusion porosimetry and X-ray CT.

7. REFERENCES

Guglielmi, Y., Birkholzer, J., Rutqvist, J., Jeanne, P., & Nussbaum, C. (2017). Can fault leakage occur before or without reactivation? Results from an in-situ fault reactivation experiment at Mont Terri. *Energy Procedia*, 114, 3167-3174.

Huo, D., Pini, R., & Benson, S. M. (2016). A calibration-free approach for measuring fracture aperture distributions using X-ray computed tomography. *Geosphere*, 12(2), 558-571.

Meredith, P., & Atkinson, B. (1985). Fracture toughness and subcritical crack growth during high-temperature tensile deformation of westerly granite and black gabbro. *Physics of the Earth and Planetary Interiors*, 796 39(1), 33-51.

Shah, S. M., Gray, F., Crawshaw, J. P. & Boek, E. S. (2016). Micro-computed tomography pore-scale study of flow in porous media: Effect of voxel resolution. *Advances in Water Resources,* 95, 276–287.

Wenning, Q. C. (2018). *Investigating Petrophysical Properties of Reservoir Rocks Using Traditional and Computerized Tomography Techniques* (Doctoral dissertation, ETH Zurich).